

Monochromatic CT Image Reconstruction from Current-Integrating Data via Deep Learning

Wenxiang Cong, Ge Wang

Abstract — In clinical CT, the energy spectrum of an x-ray source is polychromatic, and the associated x-ray detector array is currently operated in the current-integrating mode. This physical process is accurately described by the polychromatic Beer-Lambert law, which is an energy-dependent non-linear integral model and too complicated to be directly used for image reconstruction. In practice, the non-linear integral model is often approximated to a linear integral model in the form of the Radon transform, basically ignoring energy-dependent information. This model approximation would generate significant beam-hardening artifacts in a reconstructed image even after a standard correction step. In this paper, we develop a deep-learning-based CT image reconstruction method to address this challenge. Our method learns a nonlinear transformation from big data to correct measured projection data to accurately match the linear integral model along individual x-ray paths to overcome beam hardening effectively and realize monochromatic imaging in an innovative fashion. Numerical tests are performed to demonstrate the feasibility and merits of the proposed method.

Keywords — Computed tomography (CT), deep learning, Beer-Lambert law, polychromatic x-rays, beam hardening, monochromatic imaging.

I. INTRODUCTION

COMPUTED tomography (CT) is widely used for medical imaging, allowing visualization and quantification of anatomical and pathological structures with high spatial and temporal resolution. In clinical CT, the energy spectrum of an x-ray source is polychromatic, and the associated x-ray detector array is currently operated in the current-integrating mode. This physical process is accurately described by the polychromatic Beer-Lambert law, which is an energy-dependent non-linear integral model. A single set of current-integrating projection data does not allow polychromatic image reconstruction in multiple energy bins. As a result, an effective energy is assumed for the current-integrating dataset, and then a standard beam-hardening correction is performed, for example, in reference to a representative water phantom. In other words, the true physical model for CT imaging is typically avoided, which is rather complicated for either sinogram correction or image reconstruction.

Several image reconstruction methods were developed based on the non-linear integral model. De-Man et al. proposed

a maximum likelihood based reconstruction algorithm (IMPACT) [1]. This method decomposes energy-dependent attenuation coefficients of materials into linear combinations of photoelectric and Compton scattering components, and assumes a relationship between the two effects for all substances. Elbakri et al. designed a statistical image

reconstruction algorithm to reduce beam hardening artifacts [2]. Their algorithm requires a distribution of materials that are estimated by segmenting an approximately reconstructed image. These approaches involve a highly nonlinear forward model in the maximum likelihood framework, being a complicated problem of nonlinear optimization at a great computational cost.

Dual-energy CT provides complete energy-dependent information under the assumption of two basis materials, allowing monochromatic imaging and material decomposition. The attenuation coefficient image can be, in principle, presented at any energy, free from beam hardening artifacts. However, this technique requires the solution of non-linear integral equation and sufficiently incoherent measurements with two well-separate energy spectra respectively.

In practice, the polychromatic non-linear model is often approximated to a line integral model known as the Radon transform, basically discarding x-ray energy-dependent information. As a matter of fact, lower energy photons are more easily attenuated than higher energy photons, which would cause an x-ray beam to become increasingly harder as it propagates through the patient [1]. The amount of the x-ray attenuation effect is no longer linear with the material thickness. Thus, x-rays traversing different paths through an object would end up to different spectra, resulting in data inconsistencies and generating significant beam-hardening artifacts in a reconstructed image. The water correction method is often used to compensate for the beam hardening effect. This method assumes that all the materials in the scan field are water equivalent in terms of x-ray attenuation characteristics. This is often not sufficient for inhomogeneous objects such as the patient, especially in the presence of high density areas such as metal implants, potentially leading to a seriously compromised image quality [2].

Over recent years, deep learning has been extremely successful in image analysis, such as image classification, identification and segmentation [3-8]. In particular, the convolutional neural network (CNN) techniques have become popular; for example, for image denoising in low-dose CT [9, 10]. The deep learning CT denoising methods learn a function between a low-dose image patch and the corresponding patch of high quality from a large training dataset. After this training

This work was supported by the National Institutes of Health Grant NIH/NIBIB R01 EB016977 and U01 EB017140.

W. Cong and G. Wang are with the Biomedical Imaging Center, Department of Biomedical Engineering, Rensselaer Polytechnic Institute, Troy, NY 12180 USA (cong@rpi.edu, wangg6@rpi.edu).

process, CNN is used to transform a low-dose CT image to a high-quality counterpart. The deep learning for image reconstruction was also proposed to enhance image quality [11]. The deep learning method was adapted to learn a regularization transformation and parameters from big data for iterative reconstruction, complying with natural structures of medical images [12]. A novel deep residual network was designed, suppressing artifacts for limited-angle CT image reconstruction [13]. The key idea behind deep learning is not difficult to appreciate. As pointed out in the article [14], “deep-learning methods are representation-learning methods with multiple levels of representation, obtained by composing simple but non-linear modules that each transform the representation at one level into a representation at a higher, slightly more abstract level. With the composition of enough such transformations, very complex functions can be learned”.

In this paper, we propose a deep-learning-based reconstruction algorithm to solve beam-hardening artifacts in CT image reconstruction from current-integrating data. Our method generates a nonlinear transformation in the form of a deep neural network through a training process with big data. This deep learning-based transform would then be capable of correcting measured projection data to accurately match the linear integral model at a target energy level, allowing beam hardening reduction and realizing monochromatic imaging. In the next section, a detailed deep-learning-based reconstruction algorithm is proposed for monochromatic x-ray CT imaging. In the third section, key details are described for the generation of a training dataset, the architecture of our neural network, and the design of the training process. In the fourth section, representative numerical simulation results are reported and commented on. In the last section, relevant issues are discussed, key contributions are summarized, and the paper is concluded.

II. METHODOLOGY

In medical CT, the x-ray source emits a polychromatic spectrum of x-ray photons up to over 100 kVp. When polychromatic x-rays pass through the patient, the x-ray linear attenuation in the object depends on the material composition and the photon energy, the x-ray intensity after the attenuation process is measured by a current-integrating detector. The physical process can be exactly described by the non-linear integral model [15]:

$$I(l) = \int_{E_{\min}}^{E_{\max}} S(E) \exp\left(-\int_l \mu(r, E) dr\right) dE, \quad (1)$$

where $S(E)$ is the energy distribution (spectrum) of x-ray photons from the x-ray source, and $\mu(r, E)$ is the linear attenuation coefficient of the object at an energy E and a spatial position r , and $I(l)$ is the x-ray intensity measured by detector along a path l . While x-ray photons go through the object, they are statistically attenuated according to the nonlinear equation (1). According to the integral mean value

theorem, there is an energy ε_l for each x-ray path such that the following formula holds:

$$I(l) = I_0(l) \exp\left(-\int_l \mu(r, \varepsilon_l) dr\right), \quad I_0(l) = \int_{E_{\min}}^{E_{\max}} S(E) dE, \quad (2)$$

which is equivalent to

$$\int_l \mu(r, \varepsilon_l) dr = \log\left[\frac{I_0(l)}{I(l)}\right] \quad (3)$$

where $I_0(l)$ is the number of initial incident x-ray photons along the path l that can be detected without any object in the field of view. During a CT scan, x-rays traversing different paths through an object would lead to different spectra. ε_l relies on the path l ; that is, the different paths correspond to different energy levels ε_l in Eq. (3). The disagreement in these energy levels is the reason for beam hardening artifacts in a directly reconstructed CT image [16, 17].

The purpose of this paper is to establish a nonlinear relationship to transform measured projection data $\{\log[I_0(l)/I(l)]\}$ to an ideal projection data $\log[I_0(l, \varepsilon)/I(l, \varepsilon)]$ on a given energy level ε , which is defined in the detectable energy range. Let us start with the image $\mu^*(r)$ directly reconstructed from measured data $\{\log[I_0(l)/I(l)]\}$ which contains abundant information of materials along the involved x-ray paths, and set our end target as the high-quality dataset $\log[I_0(l, \varepsilon)/I(l, \varepsilon)]$ at a properly specified energy level ε . The purpose is to establish a deep learning-based map \mathcal{M}_l from the starting/initial image to the end dataset in a path-specific fashion; which means that all the image pixel values along an x-ray path in the initial image are input to the neural network for a corrected line integral value along the same path. Mathematically, the optimization model in the deep learning framework is as follows:

$$\min \sum_l \left\| \mathcal{M}_l(\mu^*(r)|r \in l) - \log\left[\frac{I_0(l, \varepsilon)}{I(l, \varepsilon)}\right] \right\| \quad (4)$$

If \mathcal{M}_l is simply taken as a geometric weighting, the generated value would be the uncorrected measurement $\{\log[I_0(l)/I(l)]\}$. If \mathcal{M}_l is sufficiently trained as a nonlinear transformation using a well-designed neural network, the energy inconsistency in projection data would be effectively corrected close to the ideal data $\log[I_0(l, \varepsilon)/I(l, \varepsilon)]$ at the energy level ε . Once the deep learning-corrected projection dataset is obtained, a beam-hardening-free image $\mu(r, \varepsilon)$ can be reconstructed using a suitable algorithm such as filtered back projection (FBP) or iterative methods (such as dictionary

learning based algorithms) based on the line integral model (Radon transform):

$$\int_l \mu(r, \varepsilon) dr = \log \left[\frac{I_0(l, \varepsilon)}{I(l, \varepsilon)} \right] \quad (5)$$

In other words, the image reconstruction process based on Eqs. (4) and (5) is able to utilize the power of deep learning to correct beam-hardening artifacts effectively (thanks to data-driven non-linear mapping), and promises to realize monochromatic CT imaging efficiently (with x-ray path specific correction).

III. TRAINING DATA AND NEURAL NETWORK

A. Training Data

A neural network for tomographic imaging must be trained with a large training dataset to optimize its performance. The training dataset may be generated from both simulation data and experimental data. The former can easily establish big data but may not be as perfect as the latter. Nevertheless, simulated big data can at least provide a pre-trained network for fine turning with experimental data. For simulation data, we utilized standard CT images in the Medical Image Library to generate x-ray-energy-dependent attenuation images. It is well known that photoelectric absorption and Compton scattering are the two dominant x-ray attenuation processes over the diagnostic energy range of 20-140 keV. The x-ray linear attenuation coefficient can be represented by [15, 18, 19]:

$$\mu(r, E) = \rho \frac{N_A}{A} (\sigma_{ph} + \sigma_{co}), \quad (6)$$

where ρ , N_A , and A are the mass density, Avogadro's number (6.022×10^{23} atom/g-atom) and atomic mass respectively. The photoelectric atomic cross section, σ_{ph} , is formulated as [20]

$$Z^4 \alpha^4 \frac{8}{3} \pi r_e^2 \sqrt{\frac{32}{\varepsilon^7}} \text{ for } \varepsilon < 1, \quad (6a)$$

where $\varepsilon = E/511 \text{ keV}$, Z is the atomic number, α is the fine-structure constant ($\approx 1/137$), and $r_e = 2.818 \text{ fm}$ is the classical radius of an electron. The Compton atomic cross section, σ_{co} , is formulated as $Z f_{kn}$, where f_{kn} is the Klein-Nishina function:

$$f_{kn}(\varepsilon) = 2\pi r_e^2 \left(\frac{1+\varepsilon}{\varepsilon^2} \left[\frac{2(1+\varepsilon)}{1+2\varepsilon} - \frac{1}{\varepsilon} \ln(1+2\varepsilon) \right] + \frac{1}{2\varepsilon} \ln(1+2\varepsilon) - \frac{1+3\varepsilon}{(1+2\varepsilon)^2} \right) \quad (6b)$$

With both photoelectric and Compton atomic cross sections, the associated linear attenuation coefficients can be expressed as the product of spatial-dependent and energy-dependent components:

$$\mu(r, \varepsilon) = a(r) p(\varepsilon) + c(r) q(\varepsilon), \quad (7)$$

where

$$a(r) = \rho Z^4 / A \quad (7a)$$

is the spatial-dependent photoelectric component,

$$c(r) = \rho Z / A \quad (7b)$$

is the spatial-dependent Compton scattering component,

$$p(\varepsilon) = N_A \alpha^4 \frac{8}{3} \pi r_e^2 \sqrt{\frac{32}{\varepsilon^7}} \quad (7c)$$

is the energy-dependent photoelectric component, and

$$q(\varepsilon) = N_A f_{kn}(\varepsilon) \quad (7d)$$

is the energy-dependent Compton scattering component.

The mass attenuation coefficient ($\frac{\mu}{\rho}$) of mixture or compound can be computed by

$$\frac{\mu}{\rho}(r) = \sum_i w_i \left[\frac{\mu}{\rho}(r) \right]_i \quad (8)$$

where w_i is the fraction by weight of the i^{th} atomic constituent, and the $[\mu/\rho]_i$ is the mass attenuation coefficient for the i^{th} element. Biological tissues are compounds from mostly light elements including hydrogen, carbon, oxygen, nitrogen, fluorine, sodium, magnesium, aluminum, silicon, phosphorus, sulfur, chlorine, argon, potassium, calcium, calcium, iron, and others. From the database at the National Institute of Standards and Technology (NIST) (<https://www.nist.gov>), we can determine the atomic number (Z), mass density (ρ), and atomic mass (A) for every pixel value in terms of the attenuation coefficients given the tissue types in the CT images. Thus, we can obtain the energy-dependent attenuation coefficients images based on Eqs. (6-8).

From the energy-dependent attenuation images, current-integrating projection datasets can be generated via x-ray Monte Carlo simulation, or a computer-assisted tomography simulation environment CatSim [21], which was developed by GE Global Research Center. CatSim incorporates polychromaticity, realistic quantum and electronic noise models, finite focal spot size and shape, finite detector cell size, and detector cross-talk for realistic simulation of the entire x-ray imaging process.

Dual-energy CT is an ideal device to generate datasets for training neural networks. Existing dual-energy CT methods include source kVp-switching, double-layer detection, dual-source gantry, and two-pass scanning. Dual-energy CT is to reconstruct images of an object from two projection datasets generated with two distinct x-ray energy spectra. It can provide more accurate attenuation quantification than conventional CT with a single x-ray energy spectrum. In the diagnostic energy range, x-ray energy-dependent attenuation can be approximated as a combination of photoelectric absorption and Compton scattering. Hence, monochromatic images can be reconstructed in image-domain or projection-domain [22] from dual-energy raw projection datasets, generating spectrally informative projection datasets [23].

B. Neural Network

A multi-layer perceptron (MLP) neural network was designed to perform deep learning based on Eq. (4). It consists of several layers, including an input layer, hidden layers, and an output layer [24]. Each layer contains multiple nodes, and each node is fully connected to the nodes in a subsequent layer. The pixel values along a path l through a reconstructed image $\mu^*(r)$ are input to nodes of the input layer. The hidden nodes make weighted linear combinations of the outputs from the previous layer. The value at every node is a composition function as follows,

$$y_k = \sum_{s=1}^N w_{s,t}^{(n)} \sigma \left[\cdots \sigma \left(\sum_{k=1}^N \left(w_{i,k}^{(2)} \sigma \left(\sum_{j=1}^N w_{i,j}^{(1)} x_j + b_i^{(1)} \right) + b_k^{(2)} \right) \right) \right] \quad (9)$$

where $\sigma(\cdot)$ is the activation function, and $w_{i,j}^{(n)}$ is the weight for the link between the i^{th} node of the current layer and the j^{th} node of the previous layer, and $b_i^{(n)}$ is the bias at the i^{th} node of the n^{th} layer. For image reconstruction, the output layer only contains a single node yielding a weighted linear combination of all the nodes on the last layer, as shown in Fig.1.

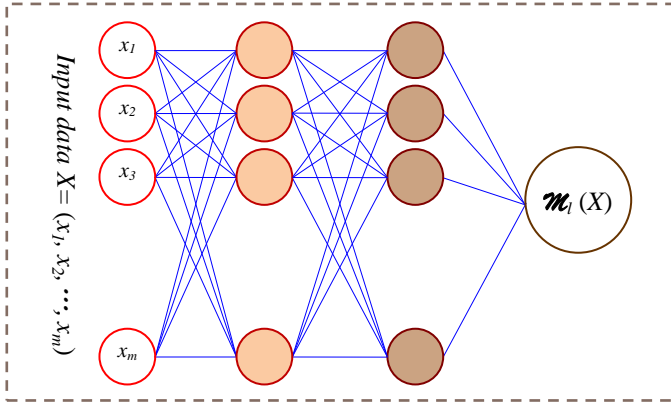


Fig.1. Multi-layer perceptron (MLP) neural network.

The optimal number of hidden layers in the MLP depends on the complexity of the function to be learned. Too few hidden layers would suffer from training errors due to under-fitting. Too many hidden layers would result in over-fitting, reducing convergence speed and network performance. The optimal number of hidden layers can be found iteratively using a heuristic method.

The MLP is a supervised learning algorithm that learns a function $\mathcal{M}_l : R^m \rightarrow R$ by training on a dataset $(X_1, Y_1), (X_2, Y_2), \dots, (X_N, Y_N)$, where X is conventional CT images, and Y is desired projection data at the specific energy level, m is dimension of the input vector. The variables in the optimization model are nonnegative weight parameters in the neural network. Moreover, the convergence speed of the neural network training significantly relies on the initial values. Main advantages of the proposed method include the simplicity due to path-specific processing and the access to good initial values. The geometric weight for the pixel values along the path l

through an image reconstructed from the directly measured projection data $\{\log[I_0(l)/I(l)]\}$ can be taken as initial values to speed up the training process and ensure the solution stability. Given an image set $X = (x_1, x_2, \dots, x_m)$ and a projection set $Y = (y_1, y_2, \dots, y_m)$, a non-linear function can be learnt for beam-hardening correction based on big data. Based on this learnt correction process, we have the following novel monochromatic image reconstruction procedure also called the Algorithm 1.

Algorithm 1

A. Input: Current-integrating projection data

B. Perform an initial image reconstruction from data using FBP

C. Learn the non-linear map for beam-hardening correction:
for each projection view

for each detector

Train the map with data

$$\mathcal{M}_l = \arg \min \sum_i \left\| \mathcal{M}_l(\mu^*(r) | r \in l) - \log \left[\frac{I_0(l, \varepsilon)}{I(l, \varepsilon)} \right] \right\|$$

end

end

D. Reconstruct an image from corrected projections

E. Output: The reconstructed image

IV. NUMERICAL SIMULATION

We performed numerical tests to evaluate the proposed deep-learning-based algorithm for monochromatic CT imaging. A set of clinical images (Mayo Clinics for “the 2016 NIH-AAPM-Mayo Clinic Low Dose CT Grand Challenge”) were used to make training data. The image dataset contains 5,936 1mm thickness full dose 512×512 CT images from 10 patients.

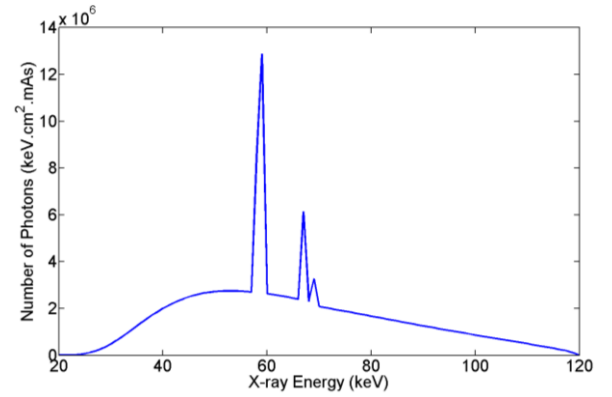


Fig. 2. Energy spectral distribution of the x-ray source simulated using the public software SpekCalc. The energy spectrum generated from the x-ray tube (120 kVp) was filtered by Aluminum of 1mm thickness and Copper of 0.3mm thickness.

Based on the method described in Section III.A, we synthesized energy-dependent linear attenuation coefficients from the reconstructed image. To characterize photoelectric and Compton cross-sections, the effective atomic numbers, densities, and atomic masses at every CT image pixel were obtained from the database in National Institute of Standards and Technology. Then, the x-ray imaging process was simulated according to the x-ray propagation forward model (polychromatic Beer-Lambert law). The energy spectra of the x-ray source were generated for the x-ray tube at 120 kVp/50mA using the public software SpekCalc [25], as shown in Fig. 2. The source-to-iso-center distance was set to 54.1 cm, while the source-to-detector distance was set to 94.9 cm. The target energy should be an effective energy (which is effectively measured) and was set to $\varepsilon = 68\text{keV}$. From energy-dependent attenuation images, mono-energy and current-integrating projection datasets were generated for 360 views over a range of 360° using the monochromatic and polychromatic Beer-Lambert formulas respectively. The projection datasets were then corrupted by Poisson noise to simulate the low-dose scan condition.

The neural network was designed to have four layers, one input layer, two hidden layers, and one output layer. The rectified Linear Unit (ReLU) was used as the activation function in the network. The neural network was trained using the stochastic gradient descent method. The backpropagation procedure computed the gradient of an objective function with respect to the weights of the multilayer network. The training procedure was programmed in Python in the TensorFlow framework, running 5,000 iterations on a computer with a NVIDIA Titan XP GPU of 12 GB memory.

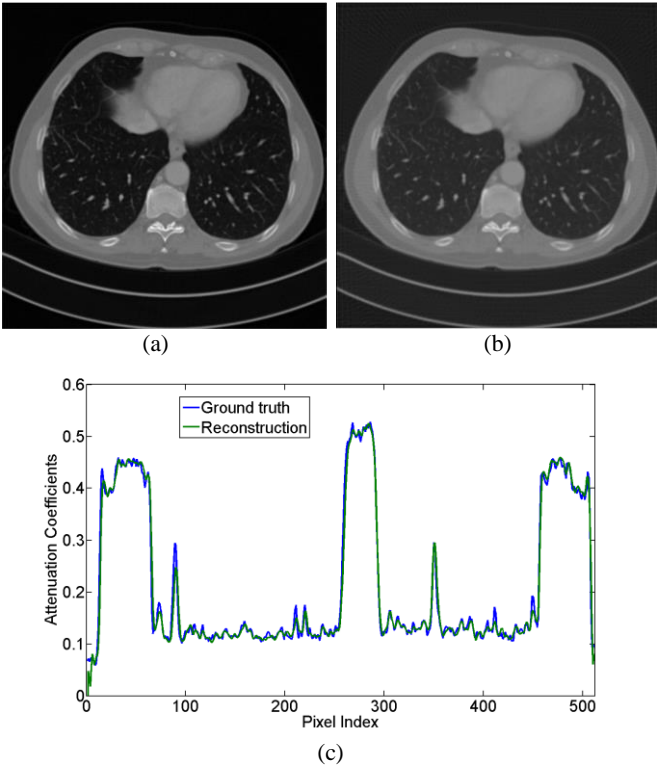


Fig. 3. Monochromatic image reconstruction. (a) The ground truth image, (b) the reconstructed image based on the deep learning based reconstruction method, and (c) profiles along the horizontal midlines in the true and reconstructed images.

To assess the performance of the trained network, using Algorithm 1 listed in Table 1, 10 datasets of raw projections were input to the trained network to generate a corrected projection data. Then, image reconstruction was performed from the corrected data. Fig. 3 (a-b) shows a comparison between the reconstructed image and the ground truth for a representative example of monochromatic image reconstruction. Fig. 3 (c) presents representative profiles along the horizontal midlines in the ground truth and reconstructed images. Also, we performed the image reconstruction based on the line integral model without beam-hardening correction. Because of the beam hardening effect, it is observed that the reconstructed image with the line integral model contains cupping artifacts, as shown in Fig. 4.

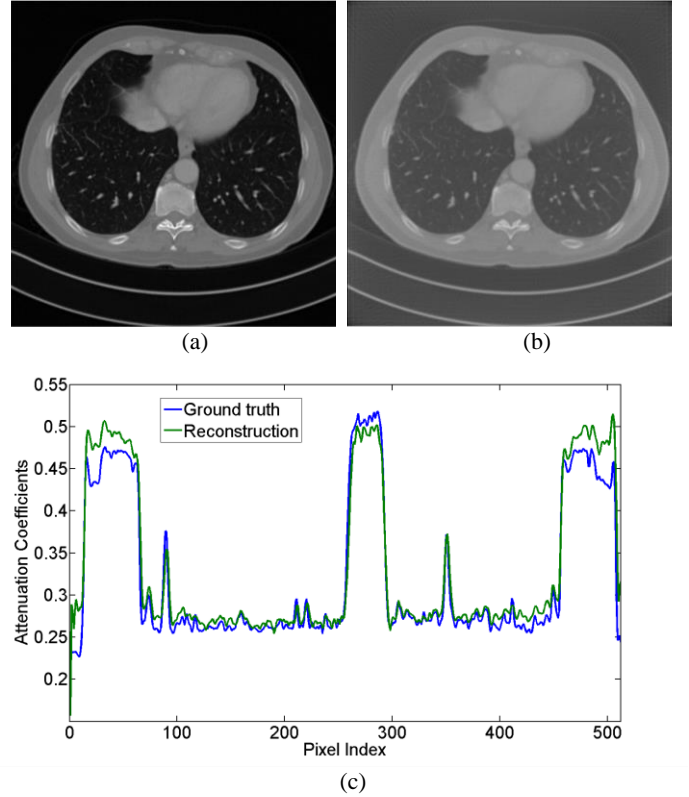


Fig. 4. Image reconstruction without beam-hardening correction. (a) The ground truth image, (b) the reconstructed attenuation image based on the linear integral model, and (c) profiles along the horizontal midlines in the true and reconstructed images.

V. DISCUSSIONS AND CONCLUSION

How big a dataset should be for it to be called big data? At the current moment, the answer is not absolutely clear since there has been no governing theory behind deep learning. However, empirical evidence and rules of a thumb are available. Suppose that the number of network parameters is N , which can be millions or more. Sontag estimated the VC dimension as a function of N for various networks (E.D. Sontag. VC dimension of neural networks. In C.M. Bishop, editor, Neural Networks and Machine Learning, pages 69-95. Springer, Berlin, 1998) [26]. A popular preference is to set the size of a

training dataset to about $N \times N$. Clearly, this can be a major challenge for deep learning in situations where labeled data are relatively few.

The above comment on the preferred size of a training dataset relative to the complexity of a neural network is actually a key to appreciate our work described in this paper. Although the number of the involved images may not be considered huge, the number of projection lines (or x-ray paths) is orders of magnitude more than the number of images. It is the number of projection lines that is equivalent to the number of training data. Also, our network takes a very limited number of pixels along each individual projection line as the input to the network so that the complexity of our network is orders of magnitude simpler than other networks used for medical imaging. Furthermore, our network targets the most fundamental level of the CT tomographic imaging workflow, and promises to utilize big data most effectively. In other words, our work is featured by its ultrahigh efficiency and effectiveness, relative to other deep learning based medical imaging techniques.

An MLP network was developed for beam-hardening correction along each and every x-ray path, which greatly facilitates subsequent image reconstruction. This scheme is not only effective but also efficient since the training programming can be implemented for all views and x-ray paths in parallel on a GPU computer. To ensure accuracy, uniqueness and stability of the solution, the training dataset should have a sufficiently high quantity of images with well-diversified features.

In the initial studies, we only used the simulation datasets to train our neural network, and already obtained encouraging results. In our on-going studies, we are augmenting our training dataset using Monte Carlo, CatSim, experimental and clinical data scanned from dual-energy CT (we are downloading these data now and hope to supplement our paper at the revision stage if we could have a chance), and optimize the network structure (number of layers, numbers of nodes, and activation functions) and parameters for further enhancement of the imaging performance. Eventually, we believe that this approach has a potential to be implemented for medical CT applications.

In conclusion, we have proposed a deep-learning-based image reconstruction method for monochromatic CT imaging when the x-ray source is polychromatic, and the x-ray detector is in the current-integrating mode. The key idea is to establish the nonlinear map between directly measured data and idealized line integrals through data-driven optimization. Due to big data based learning, the nonlinear mapping becomes a novel way to avoid the beam-hardening mechanism. Thus, the inverse Radon transform, such as filtered backprojection (FBP), can be applied for monochromatic image reconstruction with high accuracy. We are seeking real datasets to evaluate the image quality in clinical applications. The proposed method is applicable to biomedical imaging, nondestructive testing, security screening, and other applications.

REFERENCES

- [1] B. De Man, J. Nuyts, P. Dupont, G. Marchal, and P. Suetens, "An iterative maximum-likelihood polychromatic algorithm for CT," *IEEE Transactions on Medical Imaging*, vol. 20, no. 10, pp. 999-1008, Oct, 2001.
- [2] I. A. Elbakri, and J. A. Fessler, "Statistical image reconstruction for polyenergetic X-ray computed tomography," *IEEE Trans Med Imaging*, vol. 21, no. 2, pp. 89-99, Feb, 2002.
- [3] P. Danaee, R. Ghaeini, and D. A. Hendrix, "A Deep Learning Approach for Cancer Detection and Relevant Gene Identification," *Pac Symp Biocomput*, vol. 22, pp. 219-229, 2016.
- [4] F. Liu, C. Ren, H. Li, P. Zhou, X. Bo, and W. Shu, "De novo identification of replication-timing domains in the human genome by deep learning," *Bioinformatics*, vol. 32, no. 5, pp. 641-9, Mar 01, 2016.
- [5] Z. Akkus, A. Galimzianova, A. Hoogi, D. L. Rubin, and B. J. Erickson, "Deep Learning for Brain MRI Segmentation: State of the Art and Future Directions," *J Digit Imaging*, vol. 30, no. 4, pp. 449-459, Aug, 2017.
- [6] R. Gargeya, and T. Leng, "Automated Identification of Diabetic Retinopathy Using Deep Learning," *Ophthalmology*, vol. 124, no. 7, pp. 962-969, Jul, 2017.
- [7] P. Prentasac, M. Heisler, Z. Mammo, S. Lee, A. Merkur, E. Navajas, M. F. Beg, M. Sarunic, and S. Loncaric, "Segmentation of the foveal microvasculature using deep learning networks," *J Biomed Opt*, vol. 21, no. 7, pp. 75008, Jul 01, 2016.
- [8] P. Tang, X. Wang, B. Feng, and W. Liu, "Learning Multi-Instance Deep Discriminative Patterns for Image Classification," *IEEE Trans Image Process*, vol. 26, no. 7, pp. 3385-3396, Jul, 2017.
- [9] J. M. Wolterink, T. Leiner, M. A. Viergever, and I. Isgum, "Generative Adversarial Networks for Noise Reduction in Low-Dose CT," *IEEE Transactions on Medical Imaging*, pp. In press, 2017.
- [10] H. Chen, Y. Zhang, M. K. Kalra, Lin, F., Y. Chen, P. Liao, J. Zhou, and G. Wang, "Low-Dose CT with a Residual Encoder-Decoder Convolutional Neural Network (RED-CNN)," *IEEE Transactions on Medical Imaging*, pp. In press, 2017.
- [11] G. Wang, "A Perspective on Deep Imaging," *IEEE Access*, vol. 4, pp. 8914-8924, 2016.
- [12] H. Chen, Y. Zhang, Y. Chen, W. Zhang, H. Sun, Y. Lv, P. Liao, J. Zhou, and G. Wang, "Learned Experts' Assessment-based Reconstruction Network ("LEARN") for Sparse-data CT," *arXiv:1707.09636*, 2017.
- [13] J. Gu, and J. C. Ye, "Multi-Scale Wavelet Domain Residual Learning for Limited-Angle CT Reconstruction," *arXiv:1703.01382*, 2017.
- [14] Y. LeCun, Y. Bengio, and G. Hinton, "Deep learning," *Nature*, vol. 521, no. 7553, pp. 436-44, May 28, 2015.
- [15] R. E. Alvarez, and A. Macovski, "Energy-Selective Reconstructions in X-Ray Computerized Tomography," *Physics in Medicine and Biology*, vol. 21, no. 5, pp. 733-744, 1976.

[1] B. De Man, J. Nuyts, P. Dupont, G. Marchal, and P. Suetens, "An iterative maximum-likelihood polychromatic algorithm for CT," *IEEE Transactions*

- [16] T. M. Buzug, *Computed Tomography: From Photon Statistics to Modern Cone-Beam CT*: Springer-Verlag Berlin Heidelberg, 2008.
- [17] J. Hsieh, *Computed Tomography Principles, Design, Artifacts, and Recent Advances*: Wiley, 2009.
- [18] E. B. Podgoršak, *Radiation physics for medical physicists*, 2nd, enl. ed., Heidelberg: Springer, 2010.
- [19] Z. H. Qi, J. Zambelli, N. Bevins, and G. H. Chen, "Quantitative imaging of electron density and effective atomic number using phase contrast CT," *Physics in Medicine and Biology*, vol. 55, no. 9, pp. 2669-2677, May 7, 2010.
- [20] E. B. Podgorsak, *Radiation Physics for Medical Physicists*, Heidelberg: Springer, 2010.
- [21] B. De Man, S. Basu, N. Chandra, B. Dunham, P. Edic, M. Iatrou, S. McOlash, P. Sainath, C. Shaughnessy, B. Tower, and E. Williams, "CatSim: a new computer assisted tomography simulation environment," *Proc. SPIE Medical Imaging*, vol. 6510, pp. 65102G, 2007.
- [22] W. Cong, D. Harrison, Y. Xi, and G. Wang, "Image Reconstruction Method for Dual-energy Computed Tomography," *International Conference on Fully Three-Dimensional Image Reconstruction in Radiology and Nuclear Medicine*, 2017.
- [23] L. Yu, S. Leng, and C. H. McCollough, "Dual-energy CT-based monochromatic imaging," *AJR Am J Roentgenol*, vol. 199, no. 5 Suppl, pp. S9-S15, Nov, 2012.
- [24] D. Shen, G. Wu, and H. I. Suk, "Deep Learning in Medical Image Analysis," *Annu Rev Biomed Eng*, vol. 19, pp. 221-248, Jun 21, 2017.
- [25] G. Poludniowski, G. Landry, F. DeBlois, P. M. Evans, and F. Verhaegen, "SpekCalc: a program to calculate photon spectra from tungsten anode x-ray tubes," *Phys Med Biol*, vol. 54, no. 19, pp. N433-8, Oct 07, 2009.
- [26] C. M. Bishop, *Neural networks and machine learning*, Berlin ; New York: Springer, 1998.